Biochimica et Biophysica Acta 1837 (2014) 1790–1800

Contents lists available at ScienceDirect

Biochimica et Biophysica Acta

journal homepage: www.elsevier.com/locate/bbabio

Evidence of oxidative stress and mitochondrial respiratory chain dysfunction in an *in vitro* model of sepsis-induced kidney injury

C. Quoilin [a,*], A. Mouithys-Mickalad [b], S. Lécart [c], M.-P. Fontaine-Aupart [c,d], M. Hoebeke [a]

[a] Laboratory of Biomedical Spectroscopy, Department of Physics, University of Liège, 4000 Liège, Belgium
[b] Center of Oxygen Research and Development, Department of Chemistry, University of Liège, 4000 Liège, Belgium
[c] Centre de Photonique Biomédicale, CPBM/CLUPS, Fédération LUMAT, University Paris Sud, 91405 Orsay, France
[d] Institut des Sciences Moléculaires d'Orsay, CNRS and University Paris Sud, 91405 Orsay, France

ARTICLE INFO

Article history:
Received 18 April 2014
Received in revised form 29 June 2014
Accepted 5 July 2014
Available online 11 July 2014

Keywords:
Sepsis
Acute kidney injury
Mitochondrial dysfunction
Cytopathic hypoxia
Oxidative stress
Nitric oxide

ABSTRACT

To investigate the role of oxidative stress and/or mitochondrial impairment in the occurrence of acute kidney injury (AKI) during sepsis, we developed a sepsis-induced *in vitro* model using proximal tubular epithelial cells exposed to a bacterial endotoxin (lipopolysaccharide, LPS). This investigation has provided key features on the relationship between oxidative stress and mitochondrial respiratory chain activity defects.

LPS treatment resulted in an increase in the expression of inducible nitric oxide synthase (iNOS) and NADPH oxidase 4 (NOX-4), suggesting the cytosolic overexpression of nitric oxide and superoxide anion, the primary reactive nitrogen species (RNS) and reactive oxygen species (ROS). This oxidant state seemed to interrupt mitochondrial oxidative phosphorylation by reducing cytochrome c oxidase activity. As a consequence, disruptions in the electron transport and the proton pumping across the mitochondrial inner membrane occurred, leading to a decrease of the mitochondrial membrane potential, a release of apoptotic-inducing factors and a depletion of adenosine triphosphate. Interestingly, after being targeted by RNS and ROS, mitochondria became in turn producer of ROS, thus contributing to increase the mitochondrial dysfunction.

The role of oxidants in mitochondrial dysfunction was further confirmed by the use of iNOS inhibitors or antioxidants that preserve cytochrome c oxidase activity and prevent mitochondrial membrane potential dissipation. These results suggest that sepsis-induced AKI should not only be regarded as failure of energy status but also as an integrated response, including transcriptional events, ROS signaling, mitochondrial activity and metabolic orientation such as apoptosis.

1. Introduction

Sepsis is a very complex clinical condition characterized by stimulation of a systemic inflammatory response related to an infection [1,2]. This process often leads to widespread tissue injury and multiple organ dysfunction [3]. In particular, the development of acute kidney injury (AKI) is a risk factor for mortality in septic patients [4,5].

The mechanisms leading to AKI are extremely complex and still remain controversial. It was long thought that microvascular dysfunction whose net effect is a failure of oxygen delivery was likely to alter renal function at the cellular level [6]. This tissue hypoxia paradigm has been challenged by recent studies revealing that the hemodynamic mechanism might not be relevant in the pathophysiology of AKI [7,8]. It seems that the kidney is more challenged by impairment of cellular oxygen utilization rather than inadequate oxygen delivery [8–10]. This hypothesis has been corroborated in our previous work in which we have shown the incapacity of renal tubular epithelial (HK-2) cells to use adequately the available oxygen under bacterial endotoxin simulation [11].

Renal tubular epithelium seems to be no longer a passive victim of hypoxic injury [12]. Increasing number of studies suggest that it is a major site of oxidative stress, and that overproduction of reactive nitrogen species (RNS) and reactive oxygen species (ROS) may be important contributors in the mechanism of kidney injury [13–15]. These oxidants can react with cellular components, such as DNA, proteins and lipids, leading to their degradation and thereby accelerating the loss of tubular epithelium function [16,17]. However, as these studies are based on

Abbreviations: 1400W, N-(3-(aminomethyl)benzyl)acetamidine; ADP, adenosine diphosphate; AKI, acute kidney injury; ATP, adenosine triphosphate; CTRL, control; DCF, 2′-7′ dichlorofluorescin; DNA, deoxyribonucleic acid; DPI, diphenylene iodonium; EBS, ebselen (2-phenyl-1, 2-benzisoselenazol-3(2H)-one); GSH, L-glutathione; HK-2, human kidney cell lines; L-NMMA, L-N_G-monomethylarginine acetate salt; LPS, lipopolysaccharide; NAD(P)H, nicotinamide adenine dinucleotide (phosphate); NBT, nitroblue tetrazolium; ·NO, nitric oxide radical; NO_3^-, nitrate; NO_2^-, nitrite; iNOS, inducible nitric oxide synthase; NOX-4, NADPH oxidase 4; $O_2^{\bullet -}$, superoxide anion radical; $ONOO^-$, peroxynitrite anion; RNA, ribonucleic acid; RNS, reactive nitrogen species; ROS, reactive oxygen species; RT-PCR, real time polymerase chain reaction; TMRE, tetramethylrhodamine ethyl ester

* Corresponding author at: Laboratory of Biomedical Spectroscopy, Department of Physics B5a, Allée du 6 Août 17, 4000 Liège, Belgium. Tel.: +32 4 366 9568; fax: +32 4 366 3629.
E-mail address: cquoilin@ulg.ac.be (C. Quoilin).

http://dx.doi.org/10.1016/j.bbabio.2014.07.005
0005-2728/

animal models, it is difficult to dissociate direct toxicity to renal epithelial cells from side effects of renal vasoconstriction and peritubular capillary hypoperfusion.

In addition to oxidative stress, mitochondrial abnormalities have been recognized within *in vivo* and *in vitro* models. Animal models of sepsis, using either the bacterial endotoxin lipopolysaccharide (LPS) or cecal ligation and puncture as stress inducers, mainly focused on metabolic changes occurring at the level of oxidative phosphorylation. In LPS-treated rats, cytochrome c oxidase and adenosine triphosphate (ATP) synthase were down-regulated both at the transcript and protein level within 48 h after treatment [18]. This inhibition of cytochrome c oxidase was also observed in severe sepsis and had the characteristic of being irreversible [19,20]. In another case of endotoxic shock, the LPS treatment resulted in a 70% decrease of ATP levels after 8 h, a critical time for which about 30% of the animals were dead [21]. Moreover, several studies have pointed out that antioxidant treatment reversed cell mitochondrial dysfunction in sepsis animal models but there is still uncertainty concerning the involvement of ROS and RNS [22,23].

Despite this increasing evidence of oxidative stress and mitochondrial injury being important in the development of sepsis-induced AKI, it remains unclear if mitochondrial dysfunction is the primary event that leads to oxidative stress and further mitochondrial impairment, or if the oxidative stress initiates mitochondrial dysfunction with a subsequent RNS and ROS release [24,25]. In addition, the cellular source of ROS and RNS generation is still unclear. Indeed, radical species were once thought to originate almost entirely from mitochondrial metabolism but recent data focused on the crucial role of cellular enzymes, such as NADPH oxidases, as important sources of ROS [26]. This emphasizes that the mechanisms underlying ROS, RNS production and mitochondrial dysfunction have not been yet fully elucidated. To highlight this phenomenon, we developed a sepsis-induced *in vitro* model using human proximal tubular epithelial (HK-2) cells exposed to LPS. This investigation has provided key features on the relationship between oxidative stress and mitochondrial respiratory chain activity defects.

2. Materials and methods

2.1. Cell culture and treatment

HK-2 cells, an immortalized proximal tubular epithelial cell line from normal adult human kidney [27], were cultured in DMEM (Lonza, Switzerland) supplemented with 10% heat-inactivated FBS (Biochrom, Germany), 2 mM L-glutamine, 100 U/ml penicillin and 100 μg/ml streptomycin (Invitrogen, Belgium). Cells were grown to approximately 70% confluence at 37 °C in a humidified 5% CO_2 incubator.

To determine the toxic effects of LPS on mitochondrial functionality of HK-2 cells, they were incubated with fresh medium containing 1 μg/ml LPS from *Escherichia coli* 055:B5 (Sigma Aldrich, Belgium) for different incubation times. The role of oxidants was investigated by incubating cells for 6 h with fresh medium containing 1 μg/ml LPS and different types of antioxidants (all from Enzo Life Science, Belgium): 10 μM L-NMMA, 10 μM 1400W, 1 μM diphenylene iodonium (DPI), 100 μM L-glutathione (GSH), or 10 μM ebselen (EBS). For each experiment, cells were incubated without any endotoxin or drugs and taken as control groups.

2.2. Measurement of NO_2^-/NO_3^- in culture media

To investigate the implication of nitric oxide radical (•NO) in the mechanism by which LPS induced HK-2 cell stress, its production was controlled. At the end of the LPS treatment of HK-2 cells, the culture supernatants (without red phenol) were collected and the concentrations of NO_2^-/NO_3^- were quantified by using the Total Nitric Oxide Detection Kit (Enzo Life Sciences, Belgium). This assay is based on the enzymatic reduction of NO_3^- to NO_2^- by nitrate reductase. The reaction was followed by the colorimetric detection of NO_2^- as a colored azo dye, product of the Griess reaction that absorbs visible light at 540 nm. The total •NO released by cells was determined by subtracting NO_2^-/NO_3^- levels initially present in the media from the levels determined after incubation.

2.3. RT-PCR for iNOS induction

Inducible nitric oxide synthase (iNOS) is one of the major sources of •NO by catalyzing L-arginine. Its messenger RNA (mRNA) levels was estimate by RT-PCR experiments. Total RNA was purified from HK-2 cells using RNeasy Mini Kit (Quiagen, Canada) as described by the manufacturer and quantified by its UV absorbance. RNA was then reverse transcribed using the High Capacity cDNA Reverse Transcription Kit (Applied Biosystems, Canada). Specific primers from TaqMan Gene Expression Assays (Applied Biosystems, Canada) for iNOS and actin were used for amplification of cDNA using TaqMan Universal Master Mix II (Applied Biosystems, Canada). Amplification was performed by successive 40 cycles of temperature (95 °C, 15 s; 60 °C, 60 s) in a temperature cycler (DNA Thermal Cycler, Perkin-Elmer). The primers used were human β-actin (ACTB, Hs99999903_m1) and human iNOS (NOS2, Hs01075529_m1). The LPS-stimulated iNOS expression relative actin was reported as the fold increase compared to that of non-stimulated.

2.4. Quantification of $O_2^{\bullet -}$ production

As ROS are possible mediators of cell alterations, we considered the possible implication of superoxide anion radicals ($O_2^{\bullet -}$). After LPS treatment, the concentration of $O_2^{\bullet -}$ in HK-2 cells was determined by the spectrophotometric method based on the reduction of nitroblue tetrazolium (NBT) to formazan in the presence of $O_2^{\bullet -}$ [28,29]. In a 24-well plate containing HK-2 cells treated with LPS, 200 μl of 0.2% NBT solution was added for 1 h at 37 °C. After incubation, cells were washed twice with prewarmed PBS, then once with methanol in order to completely remove the extracellular formazan. NBT deposits inside cells were then dissolved with 2 M KOH and DMSO and the resulting color reaction was measured spectrophotometrically on microplate reader at 650 nm (Multiskan Microplate Reader, Thermo scientific, Belgium).

2.5. NOX-4 western blot analysis

NADPH oxidase 4 (NOX-4) is a potent source of $O_2^{\bullet -}$ in kidney [30]. Its expression in HK-2 cells during LPS treatment was detected by western blot experiments. Cellular preparations were homogenized in lysis buffer containing a mixture of protease and phosphatase inhibitors, 150 mM NaCl, 20 mM Tris, 10% glycerol, 5 mM EGTA, 5 mM EDTA, 1% Triton X-100, 0.1% SDS, and 1% sodium deoxycholate (all chemicals from Sigma-Aldrich, Canada). Samples were centrifuged at 14000 rpm, 4 °C for 10 min and the supernatant protein concentrations were determined using the BCA protein assay kit (Pierce, Canada) following the manufacturer's instructions. Samples were subjected to DTT and glycerol, boiled for 5 min and stored at −20 °C until analysis.

20 μg of proteins per well was separated on 7.5% SDS-PAGE gel and transferred to nitrocellulose membranes (materials were from Bio-Rad Laboratories — Clinical Diagnostics, Canada). After 1 h of blocking in TBS containing 0.1% Tween and 5% BSA, membranes were incubated overnight at 4 °C with primary antibodies: 0.4 μg/ml of goat polyclonal anti-NOX-4 antibody (Santa Cruz Biotechnology, sc-55142) and 1/20000 dilution of mouse anti-actin (Millipore, MAB1501). After washes, membranes were incubated for 1 h with the appropriate HRP-conjugated secondary antibody. The immunoreactive bands were detected by the enhanced chemiluminescence method and intensities were quantified using the ImageJ program.

2.6. Measurement of cytochrome c release

Cytochrome c is an essential component of the electron transport chain in mitochondria transferring one electron from complex III to complex IV. Its release to the cytoplasm is involved in initiation of cell apoptosis. Cytosolic and mitochondrial cytochrome c concentrations were measured using the double antibody sandwich ELISA kit (Enzo Life Sciences, Belgium). Briefly, HK-2 cells were treated with 1 μg/ml LPS for 1 h or 6 h, harvested, suspended in HBSS at the final concentration of 10^7 cells/ml and centrifuged at 500 ×*g* for 5 min. The pellet was incubated with Digitonin Cell Permeabilization Buffer on ice for 5 min and centrifuged at 500 ×*g*, 4 °C for 10 min. The supernatant containing the cytosolic fraction of cytochrome c (fraction 1) was kept on ice and the pellet was then incubated with RIPA Cell Lysis Buffer on ice for 5 min. The resulting lysate was centrifuged at 5000 ×*g*, 4 °C for 10 min. The supernatant containing the mitochondrial fraction of cytochrome c (fraction 2) was kept on ice. Both fractions 1 and 2 were introduced on a 96-well plate coated with a monoclonal antibody specific to cytochrome c. The appropriate antibody, conjugate and substrate were added in each well according to the kit protocol and the optical density at 405 nm was read on a Multiskan Microplate Reader (Thermo scientific, Belgium). Concentrations of cytochrome c were calculated from a standard curve.

2.7. Measurement of complex IV activity

Mitochondrial complex IV catalyzes the terminal reaction of the electron transport chain, the reduction of oxygen to water. It plays a critical role in establishing the electrical membrane potential that ATP synthase uses to synthesize ATP. The mitochondrial complex IV activity was controlled in LPS-treated HK-2 cells. After LPS treatment, HK-2 cells were collected in ice cold PBS and centrifuged at 350 ×*g*, 4 °C for 10 min. The cellular pellet was resuspended into a small amount of isolation buffer (300 mM D-Mannitol, 0.1% BSA, 250 μM EDTA, 10 mM HEPES, pH 7.4). It was homogenized for 10 min with a Dounce homogenizer and then centrifuged at 1500 *g*, 4 °C for 10 min. The supernatant, containing the cell cytosol and mitochondria, was then centrifuged at 14000 ×*g*, 4 °C for 15 min. The cytosolic supernatant was kept and the protein content was measured with a BCA protein assay kit (Sigma-Aldrich, Belgium). The mitochondrial pellet was resuspended in storage buffer (225 mM D-Mannitol, 75 mM sucrose, 125 μM EDTA, 10 mM Tris, pH 7.4) and centrifuged twice at 14000 ×*g*, 4 °C for 15 min. At the end, the preparation was resuspended in 100 μl of storage buffer and stored at −80 °C until analysis.

The mitochondrial complex IV activity was analyzed using the cytochrome c oxidase assay kit (Sigma-Aldrich, Belgium). This colorimetric assay is based on the quantification of the ferrocytochrome c absorbance decrease at 550 nm caused by its oxidation by complex IV. The kinetics was performed on a Multiskan Microplate Reader (Thermo scientific, Belgium).

2.8. Measurement of ATP content by bioluminescence

The electron transport chain, together with ATP synthase, provides the vast majority of cellular energy in the form of ATP. Its production in renal cells under LPS stimulation was controlled by using a commercially available luciferin–luciferase assay kit (Sigma-Aldrich, Belgium). HK-2 cells were treated with 1 μg/ml LPS for 1 h or 6 h, washed twice with PBS, harvested and lysed with the somatic cell ATP releasing reagent provided by the commercial kit. Luciferin substrate and luciferase enzyme were added and bioluminescence was assessed on a Fluoroskan Ascent Microplate Fluorometer (Thermo scientific, Belgium). Whole cell ATP content was determined by running an internal standard. The cellular ATP level was converted to a percentage of untreated cells.

2.9. Confocal laser scanning microscopy for fluorescence imaging

Different specific fluorescent probes (all from Molecular Probes, Life Technologies, Belgium) were used to assess mitochondrial activity and cellular oxidative stress. MitoTracker Green probe is sequestered by functioning mitochondria and is capable of staining mitochondria regardless of their polarization status; therefore it is considered as a structural dye [31,32]. The potentiometric fluorescent dye TMRE was used to control the mitochondrial membrane potential as it is known to accumulate in the mitochondrial matrix driven by the electrochemical gradient [31,33]. DCF and MitoSOX Red were used to target oxidative stress inside living cells as their oxidation by ROS was associated to green and red fluorescence respectively [31,34,35]. Cells were cultured on glass coverslips in 6-well plates and then respectively incubated at 37 °C with 100 nM MitoTracker Green and 5 μM MitoSOX Red for 20 min or 20 nM TMRE and 20 μM DCF for 10 min. Furthermore, to inhibit the complex I activity, HK-2 cells were incubated for 1 h with rotenone which blocks NADH oxidation. Prior to microscopy experiments, cells were washed three times with PBS and the coverslips were mounted on a hydrostatic Attofluor cell chamber (Invitrogen) filled with prewarmed HBSS buffer.

Fluorescence images were performed using Leica SP5-AOBS confocal laser scanning microscope (Leica, Germany) implemented at the *Centre de Photonique Biomédicale* (CPBM) of Orsay (France). Images were acquired using a 40×–1.25 numerical aperture oil immersion objective. The size of the confocal images was 512 × 512 pixels recorded on 12 bits photomultiplier with a zoom value of 1×. An UV laser (364 nm) was used as the excitation of endogenous NADH and its fluorescence was collected in the spectral range 420–480 nm. MitoTracker Green and DCF fluorescence were excited with the 488 nm wavelength of a continuous argon laser and their fluorescence was collected in the spectral range 495–535 nm. MitoSOX Red and TMRE were excited at 516 nm and 543 nm respectively and their fluorescence was collected in the spectral range 570–620 nm.

All confocal microscopy experiments were performed at least 3 times. ImageJ software was used to analyze the images, which were false color coded for display.

2.10. Co-localization experiments

For co-localization experiments, cells were observed using a 63×–1.4 numerical aperture and the zoom was optimized according to the Shannon–Nyquist theorem to obtain the best sampling regarding the resolution of the confocal microscope [36]. Thus to decipher co-localization of NADH and MitoTracker Green, we used a 7.03× zoom in order to have the most appropriate lateral pixel size $d_{xy} = 68.57$ nm with a mean emission wavelength located at 480 nm. The step of the z-stack was determined by the axial pixel size $d_z = 0.15$ μm. For co-localization experiments of MitoTracker Green and MitoSOX Red, a 6.63× zoom was used in order to have a lateral pixel size $d_{xy} =$ 73.7 nm with a mean emission wavelength located at 516 nm still with an axial pixel size $d_z = 0.15$ μm.

Co-localization analysis was performed using JACoP v2.0, a plug-in running under ImageJ software, developed by Bolte et Coredelières [36]. The statistical method provides the Pearson coefficient which varies between −1 (exclusion) and +1 (total co-localization) and reflects an unbiased co-localization of two fluorescent probes as tested by Costes' method [37,38]. In the present work, a Pearson coefficient >+0.5 was considered statistically significant for co-localization of two probes.

2.11. Flow cytometry analysis of mitochondrial activity

To control cell mitochondrial activity, flow cytometry experiments were performed using FACSCalibur flow cytometer (Becton Dickinson) equipped with a 20 mW argon ion laser tuned to 488 nm and a

photomultiplier as a detector. Data acquisition was performed using CellQuest software. After LPS exposure, HK-2 cells were washed twice with PBS and incubated with 100 nM MitoTracker Green and 5 μM MitoSOX Red for 20 min. As for confocal microscopy, cells were washed three times with PBS and resuspended in HBSS before flow cytometry analysis. The MitoTracker green fluorescence (FL1) and the MitoSOX Red fluorescence (FL2) were collected through 532/45 and 590/35 band pass filters respectively. As samples were simultaneously stained with two dyes, fluorescence compensation was set up step by step in order to avoid fluorescence emission interferences. The order of magnitude of compensation parameters was FL1 −5% FL2 and FL2 −25% FL1 (determined on single staining samples).

2.12. Flow cytometry analysis of cell apoptosis

The externalization of phosphatidylserine was performed as described before [39]. After LPS treatment, HK-2 cells were washed with PBS, trypsinized and resuspended in HEPES buffer. Cells were then stained as described by the manufacturer (Annexin-V-Fluos staining kit, Roche, Germany). Briefly, 1% v/v Annexin-V-Fluorescein (ANN) and 5% v/v propidium iodide (PI) were added to 10^6 cells and incubated for 15 min at room temperature. Analysis was done with a FACSCanto II flow cytometer (Becton Dickinson) using a 488 nm excitation. The ANN blue fluorescence (FL1) and the PI yellow fluorescence (FL2) were collected through a 515/30 and 585/42 band pass filters respectively. A minimum of 10,000 cells was analyzed for each measurement. Data acquisition was performed using FACSDiva software. Living cells are characterized by both negative fluorescence of ANN and PI (ANN−/PI−), apoptotic cells by a positive fluorescence of ANN and by either a positive or a negative fluorescence of PI (ANN+/PI− or ANN+/PI−) and necrotic cells by a negative fluorescence of ANN and a positive fluorescence of PI (ANN−/PI+).

2.13. Statistical analysis

Data were represented as mean ± SD. The paired Student *t*-test was used to compare two conditions (without and with LPS treatment) using the original data. *P* values less than 0.05 were considered statistically significant.

3. Results

3.1. LPS induces iNOS expression and •NO generation in HK-2 cells

Since induction of iNOS occurs in the kidney during sepsis [15,40] and that its derivative •NO acts as a competitive substrate with O_2 for the binding site of complex IV [41,42], we have investigated their role in the modulation of renal cell respiration. Fig. 1A shows a time-dependent induction of iNOS mRNA in HK-2 cells treated with LPS. iNOS expression began to change after 1 h of treatment and increased three times at 6 h compared to control cells ($P < 0.0001$, $n = 5$).

This variation in iNOS mRNA expression was correlated to an increase in •NO production along time (Fig. 1B), reaching 50% at 6 h ($P < 0.0001$, $n = 4$) and 70% at 24 h ($P < 0.0001$, $n = 4$) compared to control cells ($n = 6$). Importantly, the rise in •NO production stimulated by LPS was blocked by the addition of a NOS inhibitor (L-NMMA), strongly suggesting the induction of this radical from the active iNOS. The relatively low level of nitrite detected in this case suggests a possible basal production of •NO by NOS in control cells, as L-NMMA is a relatively non-selective inhibitor of all NOS isoforms.

3.2. ROS are also mediators in the propagation of LPS stress

ROS are major mediators in inflammatory processes. Their production arises from the activity of numerous enzymes, including NADPH oxidase, •NO synthase, xanthine oxidase, and the mitochondrial respiratory chain.

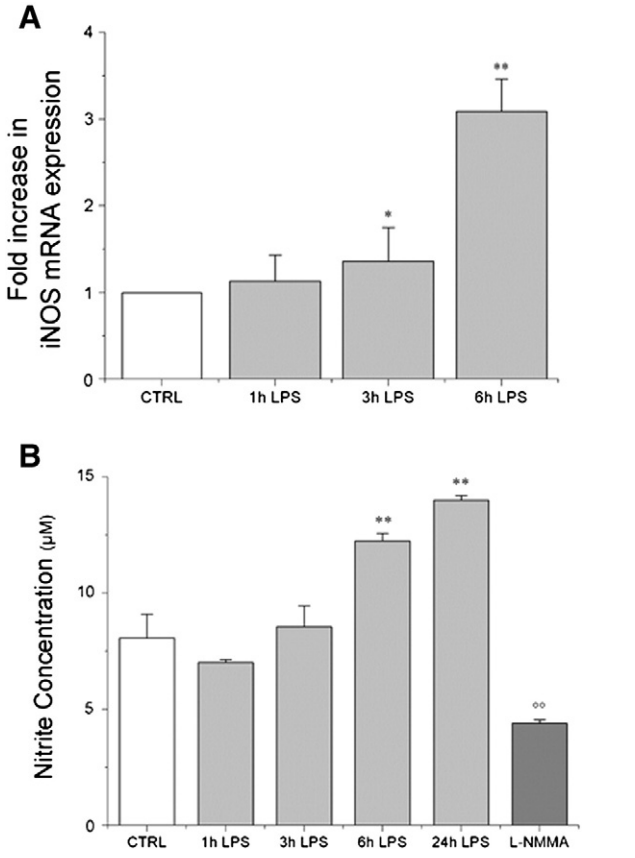

Fig. 1. Induction of iNOS and •NO generation in LPS-treated HK-2 cells. A: Time course of RT-PCR data showing induction of iNOS expression in HK-2 cells treated with LPS. B: Total •NO generation by HK-2 cells treated with LPS measured by NO_3^-/NO_2^- production in cell culture supernatants. L-NMMA (100 μM) was used as NOS-specific blocker. *, $P < 0.05$ compared to control cells; **, $P < 0.005$ compared to control cells; °°, $P < 0.005$ compared to the 6 h LPS-treated cells.

In this part, we investigated the possible role of NOX-4 in the LPS-induced intracellular oxidative stress. As shown in Fig. 2A, NOX-4 expression was already up-regulated from 3 h of LPS treatment: 1.33 ± 0.28-fold ($P = 0.008$, $n = 7$) compared to control cells and was maintained overtime: 1.34 ± 0.28-fold ($P = 0.008$, $n = 7$) and 1.36 ± 0.30-fold ($P = 0.006$, $n = 7$) after 6 h and 24 h of treatment respectively. However, this up-regulation was blocked when cells were pre-treated 2 h with 20 μM DPI, a NOX inhibitor, before LPS addition ($P = 0.03$, $n = 3$).

This increase in NOX-4 expression was accompanied by an increase in cytosolic ROS production. After 6 h and 24 h of LPS treatment, a significant rise in the DCF fluorescence signal intensity ($P < 0.0001$ and $P = 0.001$ respectively, $n = 4$) (Fig. 2B) and in the formazan absorbance ($P = 0.02$ in both cases, $n = 6$) (Fig. 2C) was observed compared to the control cells, indicating an overproduction of cellular ROS (as revealed by DCF fluorescence) and particularly superoxide anion radicals $O_2^{\bullet -}$ (as indicated by the NBT test).

When GSH and EBS, respectively ROS and peroxynitrite scavengers, were added to LPS-treated cells, the DCF fluorescence returned to a value comparable to that obtained for the untreated cells ($P < 0.0001$ and $P = 0.0004$ respectively, $n = 3$) (Fig. 2B). The same observations were made in HK-2 cells for the formazan absorbance when GSH and DPI were added to cells upon LPS treatment ($P = 0.04$ and $P = 0.02$ respectively, $n = 6$) (Fig. 2C).

3.3. LPS effects on HK-2 cell mitochondria network

The fluorescence image (Fig. 3A-a) shows that mitochondria in HK-2 cells are organized in a network with an ovoid-shaped and a multi-

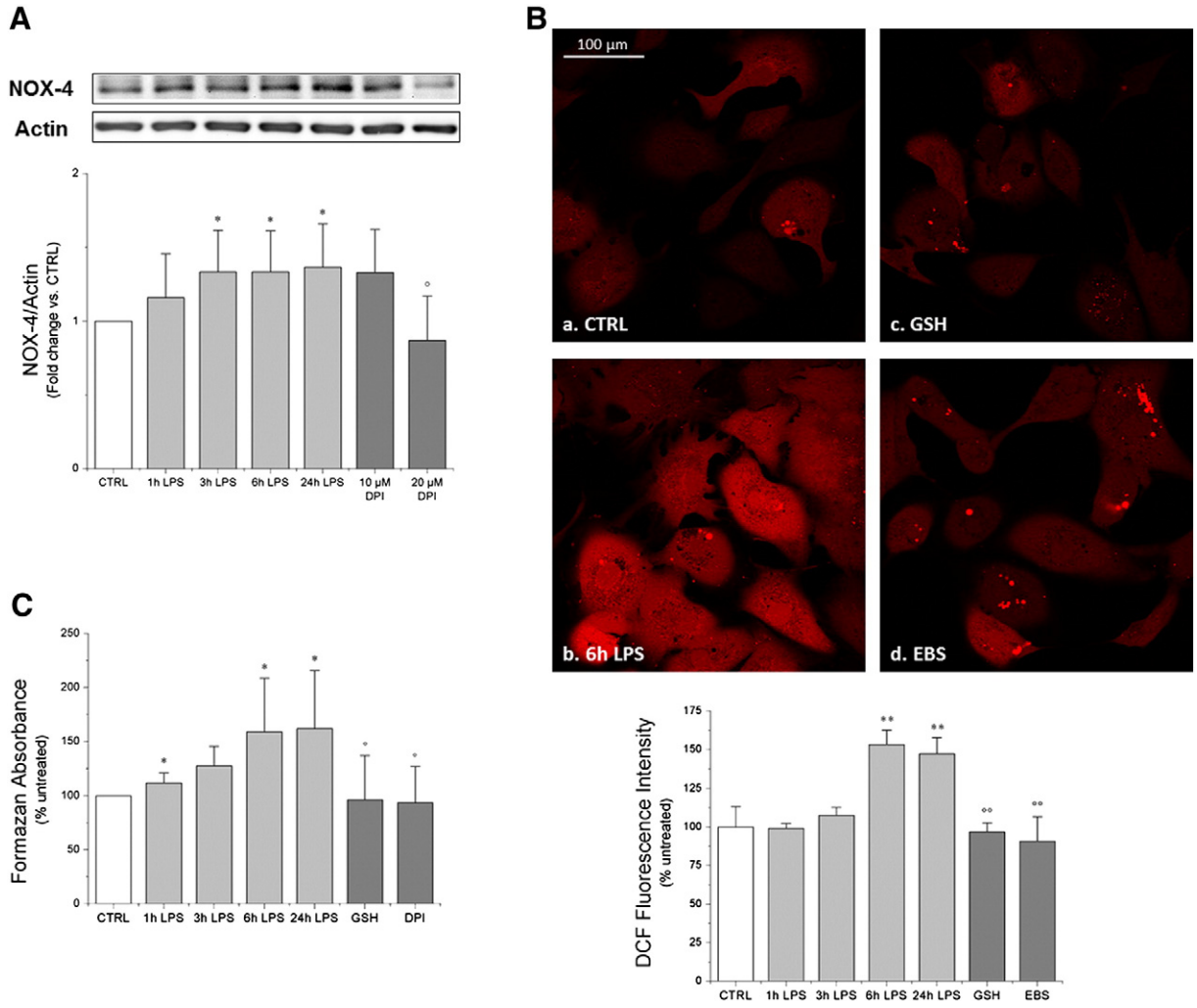

Fig. 2. Induction of NOX-4 and ROS generation in LPS-treated HK-2 cells. A: Time course of NOX-4 and actin expression in LPS-treated HK-2 cells measured by western blot. The histogram represents the densitometry analysis of NOX-4 expression relative to actin in HK-2 cells. B: Fluorescence intensity confocal images and their corresponding quantification of the DCF probe (570–620 nm) in HK-2 cells without treatment (a); after 6 h of LPS treatment (b); after 6 h of LPS treatment in presence of 100 µM GSH (c) or 10 µM EBS (d). Two hundred cells were analyzed in 3–4 independent experiments. C: Evolution of the formazan absorbance over time inside HK-2 cells. GSH (100 µM) and DPI (10 µM) were used as antioxidants and NADPH oxidase inhibitors respectively. *, $P < 0.05$ compared to control cells; **, $P < 0.005$ compared to control cells; °, $P < 0.05$ compared to the 6 h LPS-treated cells; °°, $P < 0.005$ compared to the 6 h LPS-treated cells.

branched structure. This distribution seemed not to be affected by the LPS treatment (Fig. 3A-b). The 2D quantification of the fluorescence intensity images (Fig. 3B) did not reveal significant variation in the mitochondrial fluorescence signal after LPS treatment. This was confirmed by flow cytometry analysis (Fig. 3C) that did not show any variation in the total amount of mitochondria per cell after LPS treatment whatever the incubation time.

3.4. LPS effects on the mitochondrial respiratory chain activity

The redox state of mitochondria was first controlled by monitoring the fluorescence intensity of the coenzyme nicotinamide adenine dinucleotide. Its reduced form (NADH) emits fluorescence in the 420–480 nm range while its oxidized form (NAD^+) is non-fluorescent. It is well known that in this spectral range, the cell autofluorescence emission is provided both from the mitochondrial NADH and the cytoplasmic NAD(P)H [43]. Thus we controlled that the emission collected in the 420–480 nm range originated essentially from the mitochondria of HK-2 cells. Indeed, Fig. 4A shows that NADH and MitoTracker Green fluorescence spectra overlapped (cyan points) with a Pearson coefficient of 0.75 ± 0.09 in control cells (Fig. 4A-a) and of 0.75 ± 0.07 in LPS-treated cells (Fig. 4A-b).

We then controlled that our experimental set-up allowed us to quantify a displacement of NAD^+/NADH equilibrium by using rotenone, an inhibitor of the mitochondrial electron transport chain that acts on the complex I activity. As illustrated in Fig. 4B and C, the NADH fluorescence intensity significantly increased and was correlated with both an accumulation of the reduced state of the coenzyme and an inhibition of complex I activity. However, under LPS stimulation, no variation in the intensity of NADH fluorescence signal was observed during 24 h in HK-2 cells (Fig. 4B and C).

We further assessed the LPS effects on the electron flux along the mitochondrial respiratory chain by loading HK-2 cells with MitoSOX red, a mitochondrial ROS generation indicator (Fig. 5A and B). As revealed by flow cytometry experiments (Fig. 5B), MitoSOX Red oxidation was significantly increased by 15% in LPS-treated cells only at 6 h ($P = 0.03$, $n = 4$) and 24 h ($P = 0.04$, $n = 6$) following exposure. Importantly, MitoSOX Red co-localized almost totally with MitoTracker Green probe (yellow points, Fig. 5A) with a Pearson coefficient of 0.91 ± 0.03 in control cells (Fig. 5A-a) and of 0.92 ± 0.04 in LPS-treated cells (Fig. 5A-b),

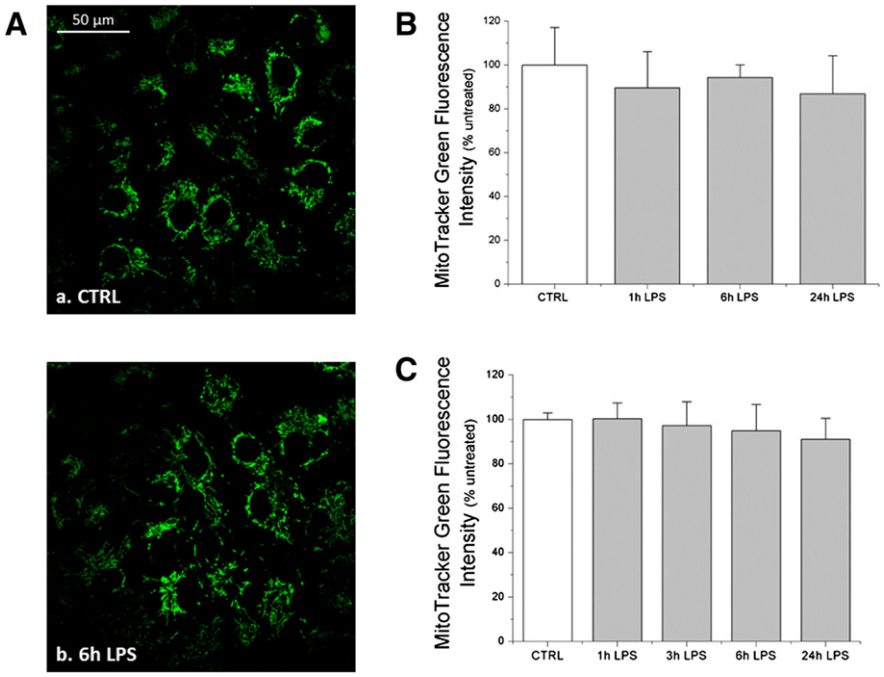

Fig. 3. Effect of LPS treatment on mitochondrial organization and quantification in HK-2 cells. A: Fluorescence intensity confocal images of the distribution of the MitoTracker dye (495–535 nm) in HK-2 cells without treatment (a) and after 6 h of LPS treatment (b). B and C: Evolution of the fluorescence signal intensity of the MitoTracker Green probe over time inside HK-2 cells measured by confocal microscopy (110 cells were analyzed in 3 independent experiments) and flow cytometry respectively.

revealing mitochondrial ROS generation. It is interesting to note that MitoSOX red fluorescence was detected within control cells, suggesting a basal production of ROS by HK-2 cell mitochondria (Fig. 5A-a). These ROS surely come from byproducts of the normal cell metabolism [44].

Cytochrome c has a major role in transferring electrons from complex III to complex IV. Its release in the cytosol could be used as an indicator of the respiratory chain dysfunction and is the primary step leading to cell apoptosis. Thereby, after LPS exposure, the amount

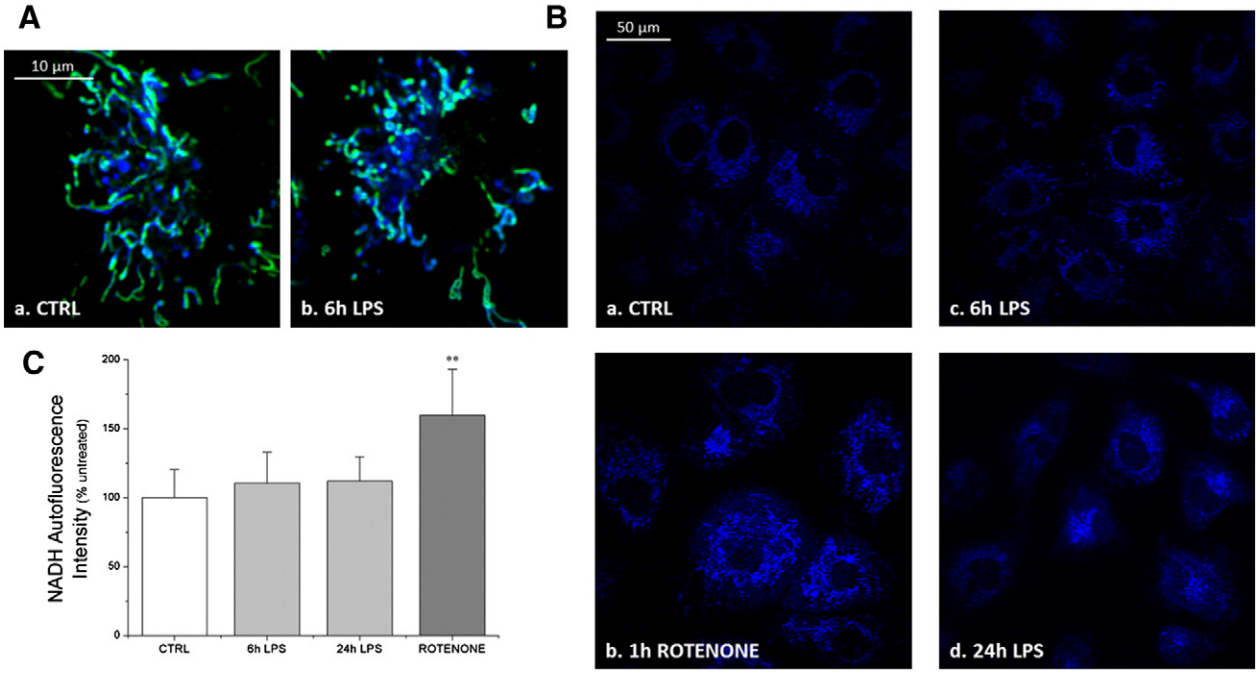

Fig. 4. Monitoring mitochondrial redox state by NADH autofluorescence measurement in HK-2 cells treated with LPS. A: Confocal microscopy imaging (7.03× zoom) of the mitochondrial network in HK-2 cells without treatment (a) and after 6 h of LPS treatment (b). The blue and green pseudo-colors of fluorescence intensity emission correspond to the emission wavelength of NADH and Mitotracker Green respectively. The sites of co-localization appear in cyan. One hundred cells were analyzed in 4 independent experiments. B: Fluorescence intensity confocal images of NADH (420–480 nm) in HK-2 cells without treatment (a); after 1 h of 1 µM rotenone treatment (b); after 6 h (c) and 24 h (d) of LPS treatment. C: Evolution of NADH autofluorescence signal intensity over time inside HK-2 cells measured by confocal microscopy. One hundred and fifty cells were analyzed in 4 independent experiments. **, $P < 0.005$ compared to control cells.

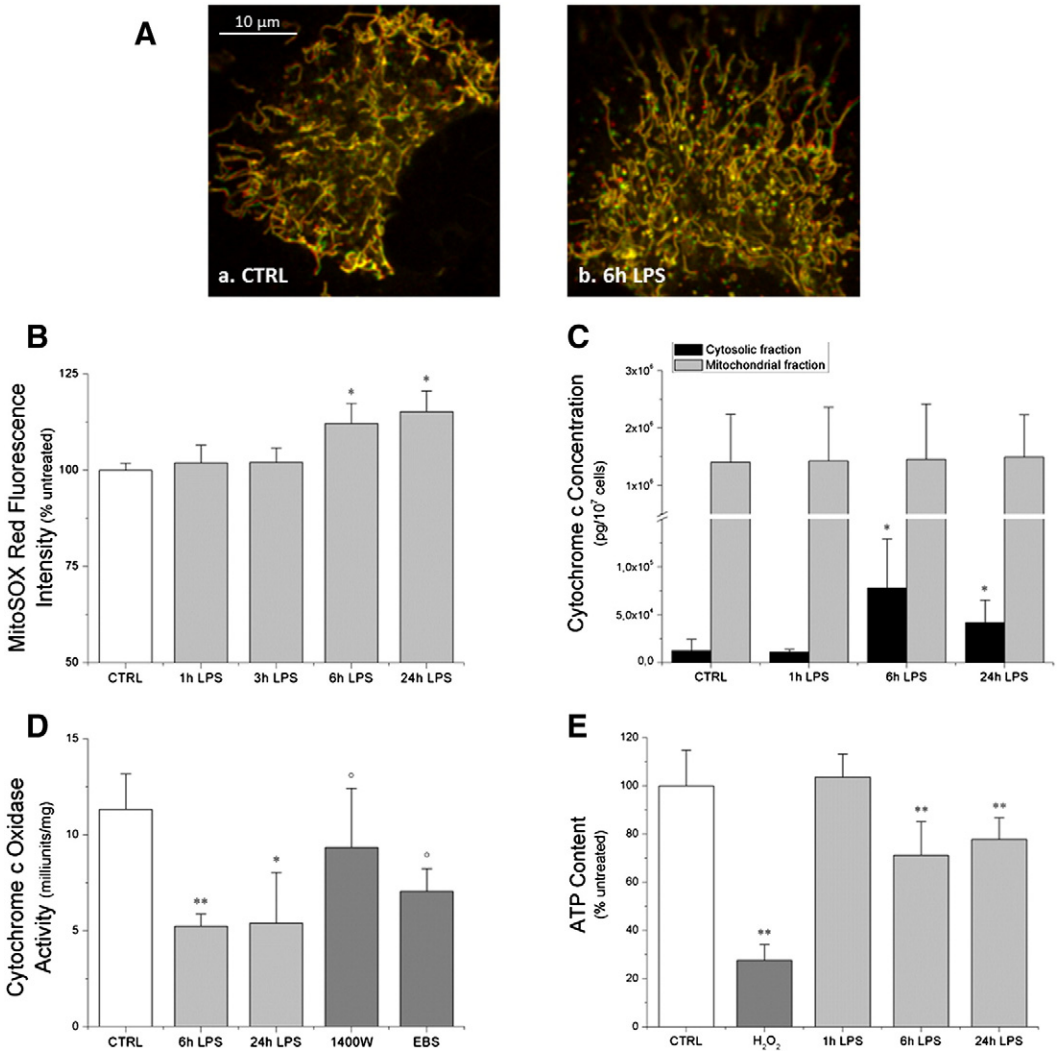

Fig. 5. Inhibitory effects of LPS on mitochondrial respiratory chain activity. HK-2 cells were treated with LPS and its impact on complexes III, IV and V was analyzed. A: Confocal microscopy imaging (6.63× zoom) of the mitochondrial network in HK-2 cells without treatment (a) and after 6 h of LPS treatment (b). The red and green pseudo-colors of fluorescence intensity emission fit to the emission wavelength of MitoSOX Red and Mitotracker Green respectively. The sites of co-localization appear in yellow. Twenty cells were analyzed in 2 independent experiments. B: Evolution of the fluorescence signal intensity of the MitoSOX Red probe over time inside HK-2 cells measured by flow cytometry. C: Respectively, cytosolic and mitochondrial cytochrome c concentrations determined by ELISA kit assay. D: Analysis of complex IV activity in LPS-treated HK-2 cells. 1400W and EBS were used as human iNOS-specific blocker and as a scavenger of peroxynitrite respectively for LPS-treated cells during 6 h. E: Determination of cellular ATP level in LPS-treated HK-2 cells. Treatment with H_2O_2 was used as a positive control group. *, $P < 0.05$ compared to control cells; **, $P < 0.005$ compared to control cells; °, $P < 0.05$ compared to the 6 h LPS-treated cells.

of cytochrome c both in the cytosol and mitochondria of HK-2 cells was determined by ELISA kit assay (Fig. 5C). The cytosolic concentration of cytochrome c was significantly increased after 6 h and 24 h of LPS treatment. Indeed, it reached $7.8 \pm 5.1 \times 10^4$ pg/10^7 cells ($P = 0.05$, $n = 4$) and $4.2 \pm 2.4 \times 10^4$ pg/10^7 cells ($P = 0.08$, $n = 3$) in the 6 h and 24 h LPS-treated cells respectively, compared to $1.3 \pm 1.2 \times 10^4$ pg/10^7 cells in control cells ($n = 4$).

Correlatively, complex IV activity dropped by 55% in HK-2 cells treated with LPS for 6 h ($P = 0.001$, $n = 4$) and 24 h ($P = 0.01$, $n = 4$). However, when the antioxidant 1400W, a selective inhibitor of human iNOS [45], or EBS was also added with LPS, complex IV activity showed a significant slight recovery (Fig. 5D). It must be noted that 1400W had more pronounced effect than EBS. Indeed, the cytochrome c oxidase activity increased from 5.2 ± 0.7 mU/mg at 6 h LPS treatment to 9.4 ± 3.1 ($P = 0.04$, $n = 4$) and 7.1 ± 102 ($P = 0.04$, $n = 4$) in the presence of 1400W and EBS respectively (Fig. 5D).

Importantly, ATP synthase activity was also inhibited by the LPS treatment of HK-2 cells, as revealed by the bioluminescent kit (Fig. 5E). A 30% fall in ATP production was observed after 6 h of treatment ($P = 0.004$, $n = 4$) and remained lower after 24 h of treatment ($P = 0.0007$, $n = 6$) by comparison to the untreated cells.

3.5. LPS induces mitochondrial membrane depolarization

Alteration of the activity of mitochondrial complexes might induce some perturbation in the electrical membrane potential created by the proton gradient across the mitochondrial inner membrane and required for ATP synthase to convert ADP to ATP.

In our experimental conditions, variations in the electrical membrane potential were detected as changes in TMRE fluorescence intensity, a membrane depolarization being correlated to TMRE fluorescence decrease [46]. This was observed after cell treatment by LPS, with a drop of the TMRE fluorescence signal of 60% at 6 h (Fig. 6A-b and B) that remained low at 24 h (Fig. 6A-c and B). This fall is clearly an indicator of mitochondrial dysfunction. However, when cells were both exposed to LPS and different antioxidants, 1400W, GSH, or EBS, the TMRE fluorescence signal intensity was not modified referring to the untreated cells (Fig. 6B).

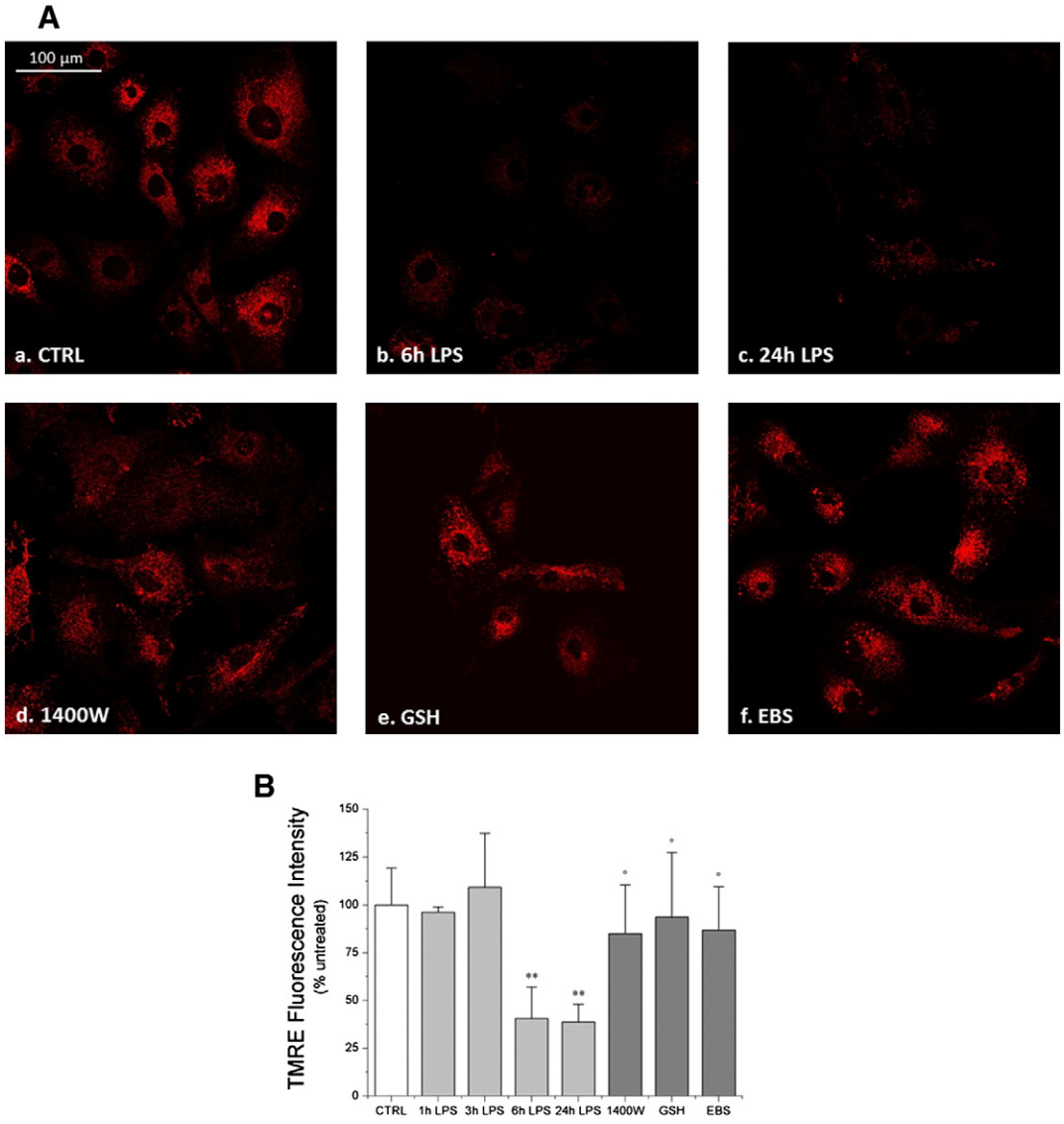

Fig. 6. Detection of mitochondrial membrane depolarization. A: Fluorescence intensity confocal images of the TMRE probe (570–620 nm) in HK-2 cells without treatment (a); after 6 h (b) and 24 h (c) of LPS treatment; after 6 h of LPS treatment in presence of 10 μM 1400W (d), 100 μM GSH (e) or 10 μM EBS (f). B: Evolution of the fluorescence signal intensity of the TMRE probe over time inside HK-2 cells measured by confocal microscopy. 1400W (10 μM), GSH (100 μM) and EBS (10 μM) were used as selective inhibitor of human iNOS, as antioxidants and as scavengers of peroxynitrite respectively. Two hundred and ten cells were analyzed in 4 independent experiments. **, $P < 0.005$ compared to control cells; °, $P < 0.05$ compared to the 6 h LPS-treated cells.

3.6. LPS and cell apoptosis

The cytochrome c release and the mitochondrial membrane potential dissipation are signs of cells undergoing apoptosis. Thereby, analysis of the percentage of necrosis/apoptosis of LPS-treated HK-2 cells was performed by following the intensity of ANN/PI labeling by flow cytometry (Fig. 7). It appeared that LPS did not induce HK-2 cell mortality during the first 24 h of treatment as the proportion of viable cells was maintained (90%). However, the proportion of apoptotic cells was significantly increased after 48 h (40%) and 72 h (55%) of LPS treatment.

4. Discussion

The mechanism of sepsis-induced kidney injury is poorly understood, in particular the link between the inflammation process and renal cell dysfunction has not been yet well established. However, for some years, it has become increasingly clear that oxidative stress and mitochondrial dysfunction are implicated in the development of sepsis-induced kidney injury but the precise pathophysiological mechanisms remain elusive [47,48]. In particular, it is not certain whether mitochondrial dysfunction is the primary event leading to oxidative stress and with subsequent mitochondrial damage or, conversely, whether oxidative stress contributes to mitochondrial dysfunction [24,25]. In a previous study, we have demonstrated that the basal respiration of renal HK-2 cells subjected to the LPS endotoxin was altered and presented a strong decrease in the oxygen consumption rates [11]. This cell metabolic down regulation strongly suggests an alteration of cellular respiration, with mitochondria probably playing a prominent role. In this context, the present study has employed HK-2 cells as a cell model system and has aimed to elucidate the mechanism of cell renal respiration dysfunction under LPS stress.

The present study reveals for the first time that the intracellular oxidative stress occurs before mitochondrial dysfunction in renal cells subjected to LPS stimulation. Indeed, our study reveals that the activation of the two enzymes, NADPH oxidase 4 (NOX-4) and inducible NO synthase (iNOS), comes out as soon as the renal cells were stressed by LPS. The rapid induction of NOX-4 and iNOS overexpression gives rise

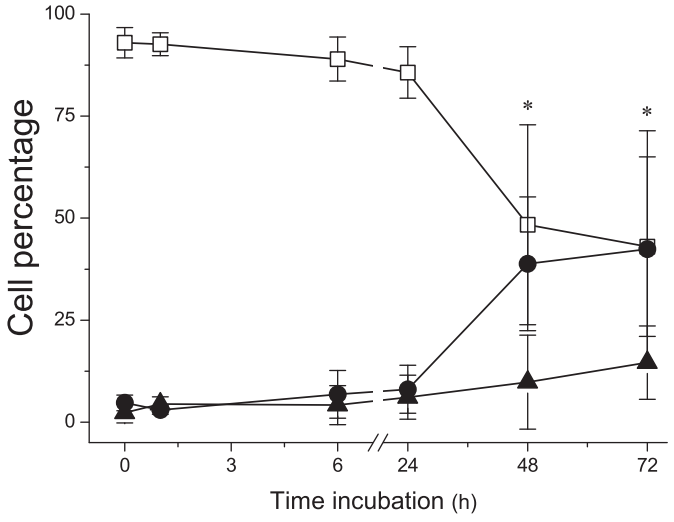

Fig. 7. Effect of LPS on HK-2 cells mortality. Percentage of living (□), apoptotic (●) and necrotic (▲) cells after LPS treatment.

to the generation of intracytosolic $O_2^{\bullet -}$ and •NO production respectively, resulting in a primary redox state. To our knowledge, it is the first time that NADPH oxidase-derived superoxide contribution is highlighted in tubular cell injury.

Moreover, the simultaneous production of $O_2^{\bullet -}$ and •NO in the cellular cytosol could certainly stimulate the formation of $ONOO^-$, as its formation rates is competitive to that of cytoplasmic SOD. This was confirmed by the significant increase in DCF fluorescence signal, blocked when using antioxidants such as L-glutathione and ebselen, revealing further reactions of $O_2^{\bullet -}$ to form its derivatives •OH and $ONOO^-$. In a previous study, the group of Mayeux et al. has already pointed out, in an *in vitro* model of renal cells treated with septic serum, the induction of intracellular iNOS expression and the production of •NO and its by-product $ONOO^-$, but the mechanism involved was not fully explained and the oxidative stress appeared to be a consequence of mitochondrial dysfunction [15,49].

Undoubtedly, cytosolic ROS ($O_2^{\bullet -}$, •OH) and RNS (•NO, $ONOO^-$) overproduction may exert deleterious effects on the function and integrity of mitochondria with further disruption of cellular oxidative ATP production [23,50]. In particular, iNOS-derived •NO acts as a competitive substrate with O_2 for the binding site in cytochrome c oxidase (complex IV) [42]. Because of its relative stability, $ONOO^-$ can diffuse through mitochondrial compartments and undergo cytotoxic reactions with complexes I, IV and V causing their inactivation [51–54]. At the same time, $O_2^{\bullet -}$ could react with and stimulate ATP-sensitive K^+ channels in the inner mitochondrial membrane [55] and •OH could undergo mitochondrial membrane lipid peroxidation [56]. In the present experimental renal model, confocal and flow cytometry experiments have demonstrated that the functional activity of mitochondria was disrupted as the LPS treatment induced a significant fall in mitochondrial membrane polarization. However, this modification did not arise with mitochondrial spatial disorganization or total amount of mitochondrial per cell loss.

We therefore tried to characterize the electron transport chain dysfunction. Complex I activity was explored by monitoring NADH mitochondrial fluorescence. This complex, which catalyzes the transfer of electrons from NADH to coenzyme Q did not seem to be affected by LPS treatment. In contrast, cytochrome c oxidase activity was significantly inhibited by LPS treatment and was accompanied by the release of cytochrome c in the cytosol. The oxidative phosphorylation dysfunction is thus augmented due to interruption of electron flux in the electron transport chain. The involvement of inhibition of complexes I and/or IV in mitochondrial dysfunction symptoms seemed to be dependent on the tissue that undergoes stress. In animal models of sepsis, complex I remained intact and complex IV was inhibited in liver cells as we observed for the renal cells while complex I and not complex IV was inhibited in brain cells [23,57].

The use of antioxidant treatment prevented inhibition of the respiratory chain complexes, especially by restoring mitochondrial membrane polarization necessary for oxidative phosphorylation. In particular, the recovery of cytochrome c oxidase activity was more important when using 1400W rather than ebselen. The former blocks simultaneously the effects of •NO and $ONOO^-$ while the latter one only affects the $ONOO^-$ production. Thus, both •NO and $ONOO^-$ seemed to play a major role in the propagation of LPS stress on mitochondria by inhibiting cytochrome c oxidase.

Interestingly, an overproduction of mitochondrial ROS was observed probing by MitoSOX fluorescence, revealing an electron leakage from the electron transport chain. Mitochondria are a major source of intracellular ROS, which are generated as a result leakage of unpaired electrons from complexes I and III and their subsequent reaction with oxygen [19]. As complex I seemed not to be affected by LPS, it can be reasonably suggested that electrons escaped mostly from complex III. However, this mitochondrial production of ROS provides a plausible explanation for not having detected the change in the redox state of NADH. The coenzyme may be oxidized by ROS byproducts, such as peroxyl and thyl radicals [56], and may not show the expected increase in its fluorescence when complex I is inhibited. The mitochondrial generation of ROS (mainly $O_2^{\bullet -}$) supposes also mitochondrial production of ONOO— that participates both in the inhibition of cytochrome c oxidase and in the release of cytochrome c in the cytosol as reported elsewhere [54]. Overall, dysfunction of the electron transport chain generated thus more ROS enhancing therefore oxidative stress and mitochondrial damage.

The flow of electrons between respiratory mitochondrial complexes I–IV provides energy to transfer protons across the inner membrane from the matrix to the intermembrane space. The resulting mitochondrial membrane potential is not only essential for ATP production but also essential to maintain the mitochondrial homeostasis. The overall LPS-induced oxidative stress and its cumulative effect on electron transport chain enzyme complexes, mentioned in the proposed mechanism scheme (Fig. 8), have resulted in a fall in the mitochondrial membrane potential and consequently in a sharp decrease of cellular ATP level. The dissipation of the proton gradient induced an uncoupling between the electron transport chain and the ATP energy production. Altogether, the decrease in cytochrome c oxidase activity and in ATP production is in accordance with our first results showing that HK-2 cells exhibit a decreased oxygen consumption rate when treated with LPS [16]. In this way, a major mechanism that could explain the inability of the renal cells to use the available oxygen for ATP production during inflammation is likely to be an interruption in oxidative phosphorylation within mitochondria, mechanism known as cytopathic hypoxia [8,58].

Finally, the release of cytochrome c induced by the mitochondrial membrane depolarization, together with the cellular ROS generation, brought about apoptosis that was observed in HK-2 cells at the later stage of LPS treatment. This cell death is another mechanism that should be taken into account in the occurrence of kidney injury [59].

5. Conclusion

In summary, this work supports the hypothesis that the inflammatory response inherent to sepsis must be considered as a direct mechanism of AKI. Under inflammatory conditions, mitochondria play a central role in the intracellular events, the reduction in cellular oxygen utilization being related to defect of cytochrome c oxidase activity. The renal injury is thus associated to a significant reduction in the capacity to generate ATP supporting the concept of mitochondrial-based cytopathic hypoxia as the main mechanism.

This investigation has also provided key features on the relationship between oxidative stress and mitochondrial respiratory chain activity defects. Firstly, it has revealed that the intracellular oxidative stress is

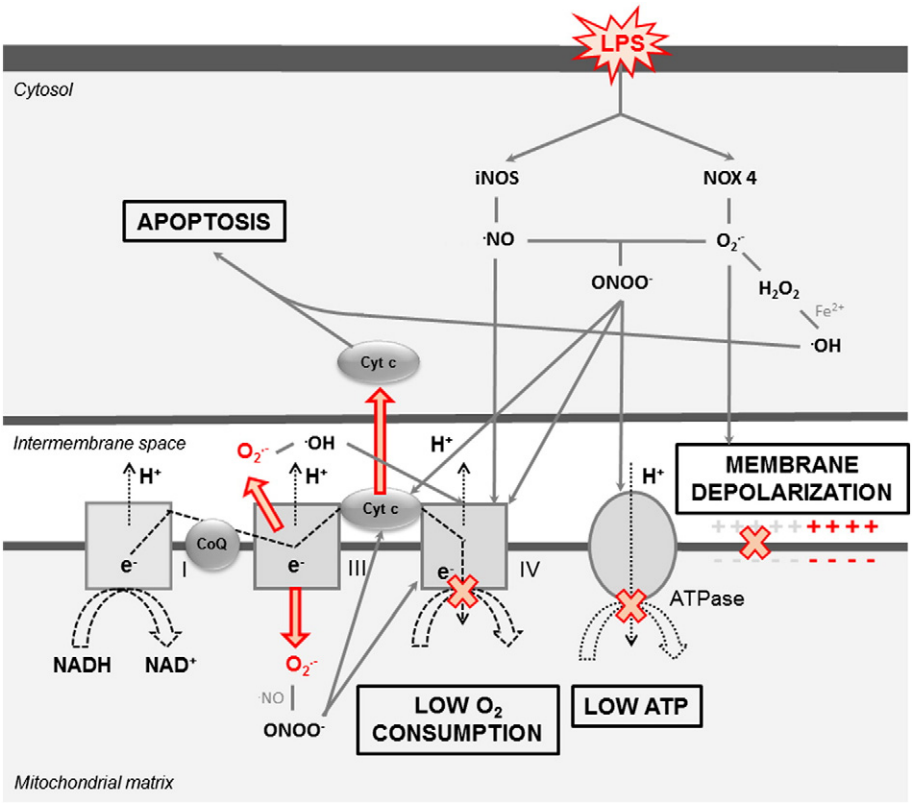

Fig. 8. Proposed mechanism of cytopathic hypoxia according to our experimental results. LPS treatment resulted in a cytosolic oxidative stress induced by the overexpression of NOX-4 and iNOS. This primary oxidant state interrupted mitochondrial oxidative phosphorylation by reducing cytochrome c oxidase activity. As a consequence, disruptions in the electron transport and the proton pumping across the mitochondrial inner membrane occurred, leading to a decrease of the mitochondrial membrane potential, a release of apoptotic-inducing factors and a depletion of cellular ATP production from ATP synthase.

an event that appears before mitochondrial dysfunction in renal cells subjected to LPS stimulation. This primary redox state is notably due to the activation of two enzymes, the NADPH oxidase 4 and the inducible NO synthase (iNOS). To our knowledge, our model reveals for the first time the role of NADPH oxidase-derived cytosolic ROS in triggering tubular cell injuries. Secondly, this study have shown that mitochondria are first target of ROS than become producer of ROS. It seems thus that a mechanism of ROS-induced ROS formation might be a main cause of the mitochondrial dysfunction.

Acknowledgements

The authors thank R. Stephan and the GIGA Imaging and Flow Cytometry platform (Liège, Belgium) for support with flow cytometry and L. Dupic for his help in the establishment of the co-localization experiments. They also thank A. Marette and K. Bellman from the laboratory of Dr. André Marette of the IUCPQ Hôpital Laval (Québec, Canada) for their expertise in western blotting and RT-PCR. They finally thank C. Ruedl from the immunology Lab of the Nanyang Technological University (Singapore) for their expertise in flow cytometry.

This work was supported by grants from the Belgian National Fund for Scientific Research (FNRS) and the University of Liège (ULg) and by grants from the International Project of Scientific Cooperation (PICS No 5991) of the French National Center for Scientific research (CNRS).

References

[1] H.B. Nguyen, D. Smith, Sepsis in the 21st century: recent definitions and therapeutic advances, Am. J. Emerg. Med. 25 (2007) 564–571.
[2] R.C. Bone, C.L. Sprung, W.J. Sibbald, Definitions for sepsis and organ failure, Crit. Care Med. 20 (1992) 724–726.
[3] S. Dickson, Sepsis and multiple organ failure, Anaesth. Intensive Care Med. 10 (2009) 165–168.
[4] R.W. Schrier, W. Wang, Acute renal failure and sepsis, N. Engl. J. Med. 351 (2004) 159–169.
[5] M. Oppert, C. Engel, F.-M. Brunkhorst, H. Bogatsch, K. Reinhart, U. Frei, K.-U. Eckardt, M. Loeffler, S. John, Acute renal failure in patients with severe sepsis and septic shock — a significant independent risk factor for mortality, Nephrol. Dial. Transplant. 23 (2008) 904–909.
[6] C. Ince, The microcirculation is the motor of sepsis, Crit. Care 9 (2005) S13–S19.
[7] C. Langenberg, R. Bellomo, C. May, L. Wan, M. Egi, S. Morgera, Renal blood flow in sepsis, Crit. Care 9 (2005) R363–R374.
[8] M.P. Fink, Bench-to-bedside review: cytopathic hypoxia, Crit. Care 6 (2002) 491–499.
[9] A. Rudiger, M. Stotz, M. Singer, Cellular process in sepsis, Swiss Med. Wkly. 138 (2008) 629–634.
[10] G. Kreymann, S. Grosser, P. Buggisch, C. Gottschall, S. Matthaei, H. Greten, Oxygen consumption and resting metabolic rate in sepsis, sepsis syndrome, and septic shock, Crit. Care Med. 21 (1993) 1012–1019.
[11] C. Quoilin, A. Mouithys-Mickalad, J. Duranteau, B. Gallez, M. Hoebeke, Endotoxin-induced basal respiration alterations of renal HK-2 cells: a sign of pathologic metabolism down-regulation, Biochem. Biophys. Res. Commun. 423 (2012) 350–354.
[12] J.M. Thurman, Triggers of inflammation after renal ischemia/reperfusion, Clin. Immunol. 123 (2007) 7–13.
[13] L. Wu, P.R. Mayeux, Effects of the inducible nitric-oxide synthase inhibitor l-N6-(1-Iminoethyl)-lysine on microcirculation and reactive nitrogen species generation in the kidney following lipopolysaccharide administration in mice, J. Pharmacol. Exp. Ther. 320 (2007) 1061–1067.
[14] L. Wu, M.M. Tiwari, K.J. Messer, J.H. Holthoff, N. Gokden, R.W. Brock, P.R. Mayeux, Peritubular capillary dysfunction and renal tubular epithelial cell stress following lipopolysaccharide administration in mice, Am. J. Physiol. Ren. Physiol. 292 (2007) F261–F268.
[15] E. Pathak, P.R. Mayeux, In vitro model of sepsis-induced renal epithelial reactive nitrogen species generation, Toxicol. Sci. 115 (2010) 475–481.
[16] H.F. Galley, Bench-to-bedside review: targeting antioxidants to mitochondria in sepsis, Crit. Care 2010 (2010) 230–238.
[17] L. Wu, N. Gokden, P.R. Mayeux, Evidence for the role of reactive nitrogen species in polymicrobial sepsis-induced renal peritubular capillary dysfunction and tubular injury, J. Am. Soc. Nephrol. 18 (2007) 1807–1815.
[18] L.A. Callahan, G.S. Supinski, Downregulation of diaphragm electron transport chain and glycolytic enzyme gene expression in sepsis, J. Appl. Physiol. 99 (2005) 1120–1126.
[19] R.J. Levy, C. Vijayasarathy, N.R. Raj, N.G. Avadhani, C.S. Deutschman, Competitive and noncompetitive inhibition of myocardial cytochrome c oxidase in sepsis, Shock 21 (2004) 110–114.

[20] E.D. Crouser, M.W. Julian, D.V. Blaho, D.R. Pfeiffer, Endotoxin-induced mitochondrial damage correlates with impaired respiratory activity, Crit. Care Med. 30 (2002) 276–284.
[21] J.C. Duvigneau, C. Piskernik, S. Haindl, B. Kloesch, R.T. Hartl, M. Huttemann, I. Lee, T. Ebel, R. Moldzio, M. Gemeiner, H. Redl, A.V. Kozlov, A novel endotoxin-induced pathway: upregulation of heme oxygenase 1, accumulation of free iron, and free iron-mediated mitochondrial dysfunction, Lab. Investig. 88 (2007) 70–77.
[22] D.A. Lowes, B.M.V. Thottakam, N.R. Webster, M.P. Murphy, H.F. Galley, The mitochondria-targeted antioxidant MitoQ protects against organ damage in a lipopolysaccharide–peptidoglycan model of sepsis, Free Radic. Biol. Med. 45 (2008) 1559–1565.
[23] P.H. Zapelini, G.T. Rezin, M.R. Cardoso, C. Ritter, F. Klamt, J.C.F. Moreira, E.L. Streck, F. Dal-Pizzol, Antioxidant treatment reverses mitochondrial dysfunction in a sepsis animal model, Mitochondrion 8 (2008) 211–218.
[24] A.J. Dare, A.R.J. Phillips, A.J.R. Hickey, A. Mittal, B. Loveday, N. Thompson, J.A. Windsor, A systematic review of experimental treatments for mitochondrial dysfunction in sepsis and multiple organ dysfunction syndrome, Free Radic. Biol. Med. 47 (2009) 1517–1525.
[25] H.F. Galley, Oxidative stress and mitochondrial dysfunction in sepsis, Br. J. Anaesth. 107 (2011) 57–64.
[26] A. Daiber, Redox signaling (cross-talk) from and to mitochondria involves mitochondrial pores and reactive oxygen species, Biochim. Biophys. Acta Bioenerg. 1797 (2010) 897–906.
[27] M.J. Ryan, G. Johnson, J. Kirk, S.M. Fuerstenberg, R.A. Zager, B. Torok-Storb, HK-2: an immortalized proximal tubule epithelial cell line from normal adult human kidney, Kidney Int. 45 (1994) 48–57.
[28] C. Hyung Sim, J. Woo Kim, C. Young-Nam, K. Chaekyun, A quantitative nitroblue tetrazolium assay for determining intracellular superoxide anion production in phagocytic cells, J. Immunoass. Immunochem. 27 (2006) 31–44.
[29] N. Esfandiari, R.K. Sharma, R.A. Saleh, A.J. Thomas, A. Agarwal, Utility of the nitroblue tetrazolium reduction test for assessment of reactive oxygen species production by seminal leukocytes and spermatozoa, J. Androl. 24 (2003) 862–870.
[30] A. Shiose, J. Kuroda, K. Tsuruya, M. Hirai, H. Hirakata, S. Naito, M. Hattori, Y. Sakaki, H. Sumimoto, A novel superoxide-producing NAD(P)H oxidase in kidney, J. Biol. Chem. 276 (2001) 1417–1423.
[31] C. Cottet-Rousselle, X. Ronot, X. Leverve, J.F. Mayol, Cytometric assessment of mitochondria using fluorescent probes, Cytometry A 79 (2011) 405–425.
[32] A. Grammenos, M. Fillet, M. Collodoro, S. Lecart, C. Quoilin, M.-P. Fontaine-Aupart, M. Hoebeke, An ESR, mass spectrometry and fluorescence microscopy approach to study the stearic acid derivatives anchoring in cells, Appl. Magn. Reson. 43 (2012) 311–320.
[33] A. Rasola, M. Geuna, A flow cytometry assay simultaneously detects independent apoptotic parameters, Cytometry 45 (2001) 151–157.
[34] P. Mukhopadhyay, M. Rajesh, G. Haskó, B.J. Hawkins, M. Madesh, P. Pacher, Simultaneous detection of apoptosis and mitochondrial superoxide production in live cells by flow cytometry and confocal microscopy, Nat. Protoc. 2 (2007) 2295–2301.
[35] P. Mukhopadhyay, M. Rajesh, K. Yoshihiro, G. Haskó, P. Pacher, Simple quantitative detection of mitochondrial superoxide production in live cells, Biochem. Biophys. Res. Commun. 358 (2007) 203–208.
[36] S. Bolte, F.P. Cordelières, A guided tour into subcellular colocalization analysis in light microscopy, J. Microsc. 224 (2006) 213–232.
[37] S.V. Costes, D. Daelemans, E.H. Cho, Z. Dobbin, G. Pavlakis, S. Lockett, Automatic and quantitative measurement of protein–protein colocalization in live cells, Biophys. J. 86 (2004) 3993–4003.
[38] E. Manders, J. Stap, G. Brakenhoff, R. van Driel, J. Atten, Dynamics of three-dimensional replication patterns during the S-phase, analysed by double labelling of DNA and confocal microscopy, J. Cell Sci. 103 (1992) 857–862.
[39] P.-H. Guelluy, M.-P. Fontaine-Aupart, A. Grammenos, S. Lécart, J. Piette, M. Hoebeke, Optimizing photodynamic therapy by liposomal formulation of the photosensitizer pyropheophorbide-a methyl ester: in vitro and ex vivo comparative biophysical investigations in a colon carcinoma cell line, Photochem. Photobiol. Sci. 24 (2010) 1252–1260.
[40] L. Wu, P.R. Mayeux, Effects of the inducible nitric-oxide synthase inhibitor L-N 6-(1-iminoethyl)-lysine on microcirculation and reactive nitrogen species generation in the kidney following lipopolysaccharide administration in mice, J. Pharmacol. Exp. Ther. 320 (2007) 1061–1067.
[41] M. Brunori, A. Giuffrè, E. Forte, D. Mastronicola, M.C. Barone, P. Sarti, Control of cytochrome c oxidase activity by nitric oxide, Biochim. Biophys. Acta Bioenerg. 1655 (2004) 365–371.
[42] G.C. Brown, Regulation of mitochondrial respiration by nitric oxide inhibition of cytochrome c oxidase, Biochim. Biophys. Acta Bioenerg. 1504 (2001) 46–57.
[43] A. Mayevsky, B. Chance, Oxidation–reduction states of NADH in vivo: from animals to clinical use, Mitochondrion 7 (2007) 330–339.
[44] P. Venditti, L. Di Stefano, S. Di Meo, Mitochondrial metabolism of reactive oxygen species, Mitochondrion 13 (2013) 71–82.
[45] E.P. Garvey, J.A. Oplinger, E.S. Furfine, R.J. Kiff, F. Laszlo, B.J.R. Whittle, R.G. Knowles, 1400W is a slow, tight binding, and highly selective inhibitor of inducible nitric-oxide synthase in vitro and in vivo, J. Biol. Chem. 272 (1997) 4959–4963.
[46] J. Plášek, A. Vojtíšková, J. Houštěk, Flow-cytometric monitoring of mitochondrial depolarisation: from fluorescence intensities to millivolts, J. Photochem. Photobiol. B Biol. 78 (2005) 99–108.
[47] J. Himmelfarb, E. McMonagle, S. Freedman, J. Klenzak, E. McMenamin, P. Le, L.B. Pupim, T.A. Ikizler, T.P. Group, Oxidative stress is increased in critically ill patients with acute renal failure, J. Am. Soc. Nephrol. 15 (2004) 2449–2456.
[48] W. Wang, S. Jittikanont, S.A. Falk, P. Li, L. Feng, P.E. Gengaro, B.D. Poole, R.P. Bowler, B.J. Day, J.D. Crapo, R.W. Schrier, Interaction among nitric oxide, reactive oxygen species, and antioxidants during endotoxemia-related acute renal failure, Am. J. Physiol. Ren. Physiol. 284 (2003) F532–F537.
[49] E. Pathak, L.A. MacMillan-Crow, P.R. Mayeux, Role of mitochondrial oxidants in an in vitro model of sepsis-induced renal injury, J. Pharmacol. Exp. Ther. 340 (2012) 192–201.
[50] E.D. Crouser, Mitochondrial dysfunction in septic shock and multiple organ dysfunction syndrome, Mitochondrion 4 (2004) 729–741.
[51] R. Radi, M. Rodriguez, L. Castro, R. Telleri, Inhibition of mitochondrial electron transport by peroxynitrite, Arch. Biochem. Biophys. 308 (1994) 89–95.
[52] M.A. Sharpe, C.E. Cooper, Interaction of peroxynitrite with mitochondrial cytochrome oxidase: catalytic production of nitric oxide and irreversible inhibition of enzyme activity, J. Biol. Chem. 273 (1998) 30961–30972.
[53] J. Boczkowski, C. Lisdero, S. Lanone, A. Samb, M. Carreras, A. Boveris, M. Aubier, J. Poderoso, Endogenous peroxynitrite mediates mitochondrial dysfunction in rat diaphragm during endotoxemia, FASEB J. 13 (1999) 1637–1646.
[54] R. Radi, A. Cassina, R. Hodara, C. Quijano, L. Castro, Peroxynitrite reactions and formation in mitochondria, Free Radic Biol Med 33 (2002) 1451–1464.
[55] R.P. Brandes, Triggering mitochondrial radical release: a new function for NADPH oxidases, Hypertension 45 (2005) 847–848.
[56] B. Halliwell, J. Gutteridge, Free Radicals in Biology and Medicine, Oxford University Press, New York, 1999.
[57] C. Comim, G. Rezin, G. Scaini, P. Di-Pietro, M. Cardoso, F. Petronilho, C. Ritter, E. Streck, J. Quevedo, F. Dal-Pizzol, Mitochondrial respiratory chain and creatine kinase activities in rat brain after sepsis induced by cecal ligation and perforation, Mitochondrion 8 (2008) 313–318.
[58] A. Harrois, O. Huet, J. Duranteau, Alterations of mitochondrial function in sepsis and critical illness, Curr. Opin. Anaesthesiol. 22 (2009) 143–149.
[59] A. Ortiz, P. Justo, A. Sanz, C. Lorz, J. Egido, Targeting apoptosis in acute tubular injury, Biochem. Pharmacol. 66 (2003) 1589–1594.